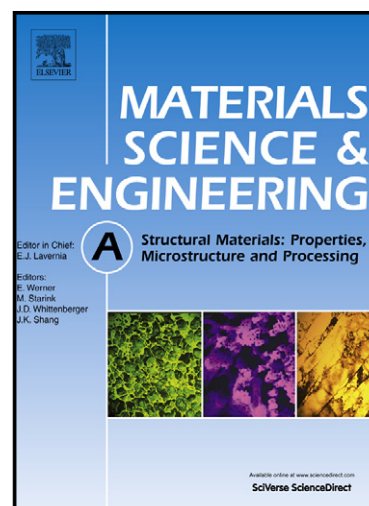# Author's Accepted Manuscript

Hot Deformation Behavior, Dynamic Recrystallization, and Physically-Based Constitutive Modeling of Plain Carbon Steels

Sepideh Saadatkia, Hamed Mirzadeh, Jose-Maria Cabrera

MATERIALS SCIENCE & ENGINEERING

A

Structural Materials: Properties, Microstructure and Processing

ELSEVIER

Editor in Chief:
E.J. Lavernia

Editors:
E. Werner
M. Starink
J.D. Whittenberger
J.K. Shang

Available online at www.sciencedirect.com
SciVerse ScienceDirect

www.elsevier.com/locate/msea

Cite this article as: Sepideh Saadatkia, Hamed Mirzadeh, Jose-Maria Cabrera, Hot Deformation Behavior, Dynamic Recrystallization, and Physically-Based Constitutive Modeling of Plain Carbon Steels, *Materials Science & Engineering A,* http://dx.doi.org/10.1016/j.msea.2015.03.104

Hot Deformation Behavior, Dynamic Recrystallization, and Physically-Based Constitutive Modeling of Plain Carbon Steels

Sepideh Saadatkia [a], Hamed Mirzadeh [a,*], Jose-Maria Cabrera [b,c]

[a] School of Metallurgy and Materials Engineering, College of Engineering, University of Tehran, P.O. Box 11155-4563, Tehran, Iran

[b] Departamento de Ciencia de los Materiales e Ingeniería Metalúrgica, ETSEIB, Universitat Politècnica de Catalunya, Av. Diagonal 647, 08028 Barcelona, Spain

[c] Fundació CTM Centre Tecnologic, Pl. de la Ciencia, 08243, Manresa, Spain

Abstract

The high-temperature deformation behaviors of low and medium carbon steels with respectively 0.06 and 0.5 wt.% C were investigated under strain rate and temperature ranges of 10^{-4}-10^{-1} s^{-1} and of 900-1100 °C. Three types of dynamic recrystallization (DRX) flow behaviors were identified, namely single peak, multiple transient steady state, and cyclic behaviors. The normalized critical stress (and strain) for the low and medium carbon steels were about 0.846 (0.531) and 0.879 (0.537), respectively. For both steels, the apparent deformation activation energy and the power of the hyperbolic sine law were found to be near the lattice self-diffusion activation energy of austenite (270 kJ/mol) and 4.5, respectively. As a result, it was concluded that the flow stress of plain carbon steels during hot deformation is mainly controlled by dislocation climb, and based on physically-based constitutive analysis, it was found that carbon has a slight effect on the hot flow stress of plain carbon steels. The significance of the approach used in this work was shown to be its reliance on the theoretical analysis based on the deformation mechanisms, which makes the comparison more reliable.

Keywords: Hot working; Constitutive equations; Dynamic recrystallization; Deformation mechanism.

* Corresponding author. Tel.: +982182084127; Fax: +982188006076.
  E-mail address: hmirzadeh@ut.ac.ir (H. Mirzadeh).

1. Introduction

Deformation temperature, strain rate, strain and interpass times must be carefully monitored to achieve required shape, microstructure, and mechanical properties. During hot working, dynamic recovery (DRV) and dynamic recrystallization (DRX) are the restoration phenomena that significantly affect the flow behavior. Due to the low stacking fault energy of austenite, the kinetics of DRV is slow and hence the DRX process normally occurs during hot forming of steels, which initiates at a critical strain (ε_c). Generally, three types of DRX flow curves have been proposed: single peak [1], multiple transient steady state (MTSS) [2,3], and cyclic [4,5] behaviors, which are dependent on the level of flow stress (deformation temperature and strain rate) and initial grain size [6]. The understanding of the hot deformation behavior together with the constitutive relations describing material flow is a prerequisite for large-scale production in the industry. The constitutive modeling of flow stress is thus important in forming processes because any feasible mathematical simulation needs accurate flow description [7-9].

Carbon is the most important alloying element in steels, which controls their microstructure and properties. Therefore, characterizing the effect of carbon on hot working behavior of steels is of special importance. For instance, its effects on the initiation of DRX, type of DRX flow curves, and hot strength of steels is essential in production of steel parts. To investigate the effect of carbon, it is logical to consider plain carbon steels with different carbon contents. In the current work, an attempt has been made to fundamentally enlighten these points based on the physically-based constitutive modeling, which result to a more reliable comparison. Indeed, on the experimental front, this problem has studied before, as will be discussed in the results and discussion section, but the obtained results seems to be contradictory as some researchers have concluded that increasing the amount of carbon promotes hardening while some others have observed a reverse trend [10-14].

2. Experimental details

The chemical composition of the studied low carbon (0.06 wt.%) and medium carbon (0.5 wt.%) steels are shown in Table 1. Uniaxial hot compression tests were performed on cylindrical samples with the height of 11.4 mm and diameter of 7.6 mm. The strain rate and temperature for this work were in the range of 10^{-4}-10^{-1} s^{-1} and 900-1100 °C, respectively. Samples were soaked at 1100 °C for 15 min before the compression test and argon flow was employed to inhibit decarburization of the steels and oxidation of the machine tools. The initial grain size measured after quenching the as-received materials form the austenitization condition were ~ 78 µm and ~ 53 µm for the medium carbon and low carbon steels, respectively. More information about the experiments and preliminary hot deformation behaviors can be found elsewhere [15]. Here, the results are revisited on the basis of improved constitutive description and analysis of the work hardening rates.

Table 1: Chemical compositions (wt.%) of the studied plain carbon steels.

Element	C	Mn	Si	P	S	Cu
Low Carbon Steel	0.06	0.42	0.12	0.002	0.005	0.13
Medium Carbon Steel	0.50	0.68	0.2	0.002	0.038	0.28

3. Results and discussion

3.1. DRX flow behavior

The stress-strain (σ-ε) curves at various conditions for both steels are shown in Fig.1. As can be seen, all three types of DRX flow curves can be identified: single peak, multiple transient steady state (MTSS), and cyclic behaviors.
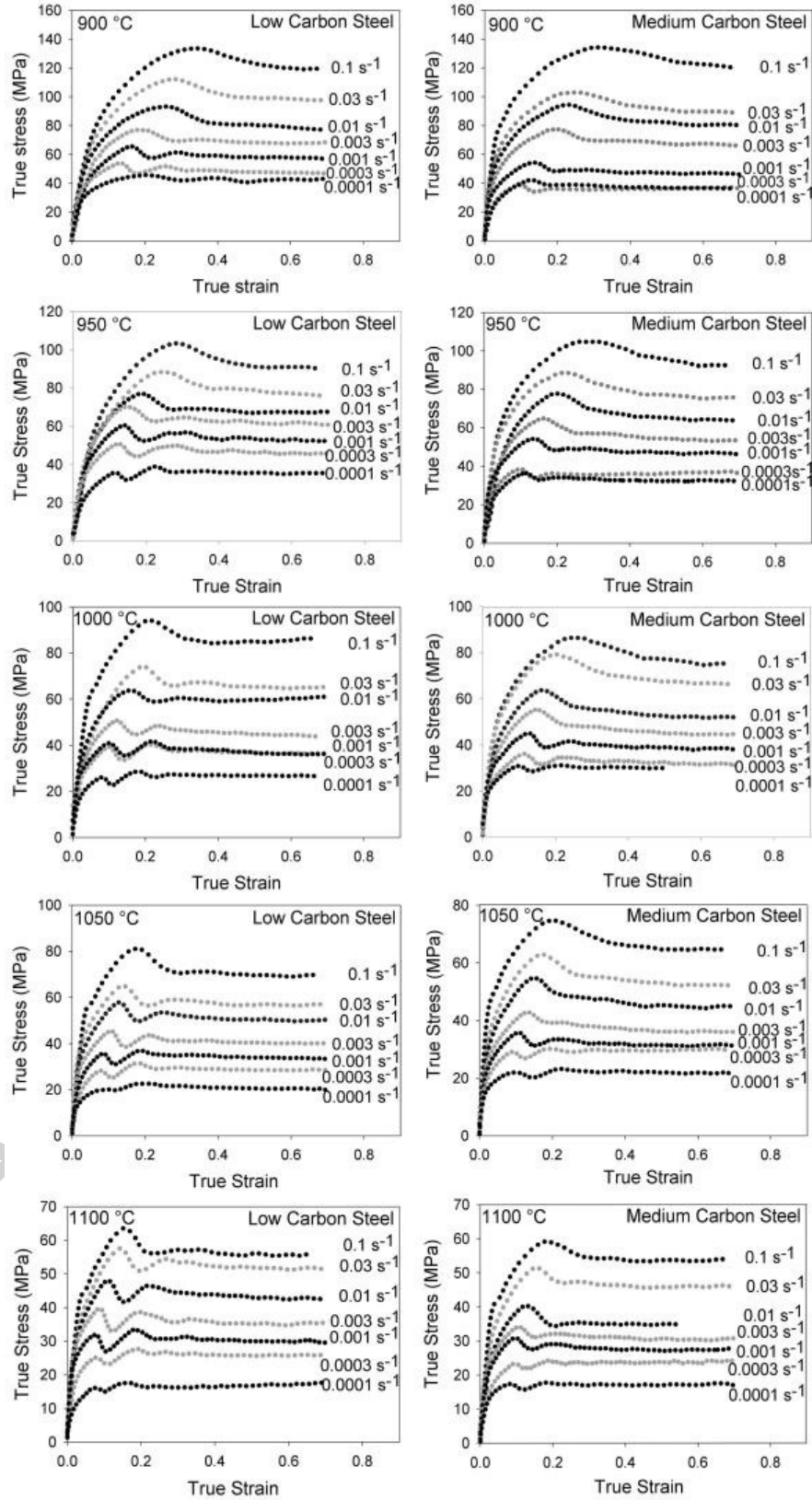
Fig. 1: Flow curves obtained at different deformation conditions.

At high strain rates and low temperatures, the shape of flow curves can be characterized as single peak behavior. In this type, more cycles of DRX initiate before the completion of the first one and the averaged flow stress of different grains will be in the form of a smooth peak. Moreover, the peak and steady state stresses decrease with an increase in the forming temperature or a decrease in strain rate. Conversely, at low strain rates and high temperatures, a multiple peak (cyclic) behavior can be noticed, in which the repetition of stress fluctuations are observed before the onset of steady state in the flow curves. This fact is attributed to the occurrence of several independent cycles of DRX. Furthermore, there are signs of another type of DRX flow curves, which can be considered as a transition state between single and cyclic behaviors. For instance, as can be seen in Fig. 2 for the deformation condition of 1050 °C - 0.003 s^{-1}, several plateaus (horizontal stress lines) followed by a decrease in flow stress after each plateau can be detected beyond the peak stress of the flow curve. Each plateau represents a transient steady state period (similar to a peak point), and the decrease in flow stress after each plateau may be attributed to the progress of a new DRX cycle. This condition was also observed in a stainless steel alloy and subsequently was named as multiple transient steady state (MTSS) behavior [2,3]. This implies that the MTSS behavior might be a general flow behavior.
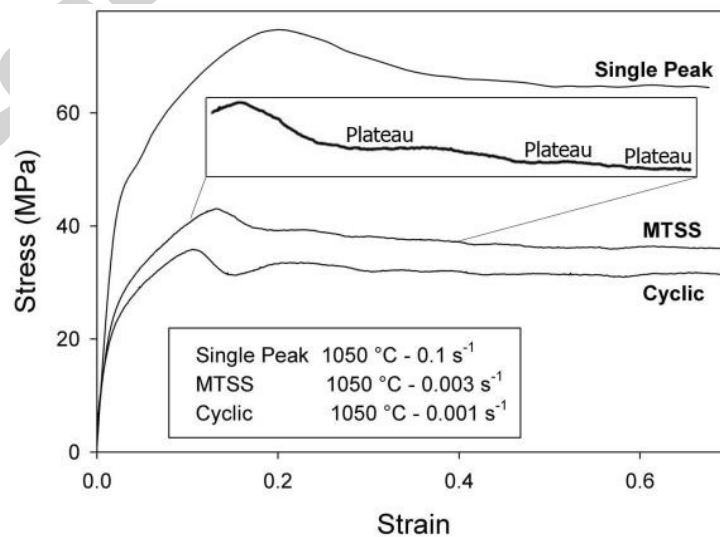

Fig. 2: Representation of different DRX flow curves for the medium carbon steel.

3.2. Work hardening rate analysis

The critical stresses for initiation of DRX (σ_C) were obtained from the inflection points in the work hardening rate ($\theta = d\sigma/d\varepsilon$) versus flow stress ($\sigma$) curves (before the peak stress) or from the minimums in the $-d\theta/d\sigma$ versus σ curves [16,17]. The former plots were used to determine other characteristic stresses. The critical strains for the onset of DRX (ε_c) were found directly from the inflection points of the $\ln\theta$-ε curves while other characteristic strains were determined from the θ-ε curves. More details are shown in Fig. 3. To obtain the values of θ, the following incremental equation was used:

$$\theta\big|_i = \frac{d\sigma}{d\varepsilon}\bigg|_i = \frac{\sigma\big|_{i+1} - \sigma\big|_{i-1}}{\varepsilon_{i+1} - \varepsilon_{i-1}} \tag{1}$$

Fig. 4 shows the relations among the various characteristic points of flow curves for both steels. Regression analysis of these curves (using an equation of the form of $y = ax$ based on the expected relations between the characteristic points) shows that $\sigma_C = 0.879\sigma_P$, $\varepsilon_C = 0.537\varepsilon_P$, and $\sigma_S = 0.875\sigma_P$ for the medium carbon steel and $\sigma_C = 0.846\sigma_P$, $\varepsilon_C = 0.531\varepsilon_P$, and $\sigma_S = 0.886\sigma_P$ for the low carbon steel. An interesting finding is the independency of the σ_C/σ_P and $\varepsilon_C/\varepsilon_P$ ratios on the carbon content. However, this does not mean that the level of σ_C, σ_P, ε_C or ε_P does not depend on the carbon content, as will be discussed later. Moreover, it can be seen that the normalized critical strain can be expressed as $\varepsilon_C / \varepsilon_P \approx 0.53$ for both steels. At the onset of steady state flow, as a result of the balance between work hardening and restoration processes, the flow stress reaches the value of $\sim 0.88\sigma_P$ for both steels. This implies that the restoration processes can effectively soften the alloy during hot working. The obtained value of normalized critical strain is also consistent with previous studies (mainly on steels) which have reported a value in the range of 0.3-0.9 [3]. The normalized critical strain of ~ 0.53 is lower than the one reported for medium carbon microalloyed steel (~ 0.62) [18], which reveals that carbon does not significantly affect this value but the microalloying elements are effective in retardation of recrystallization.
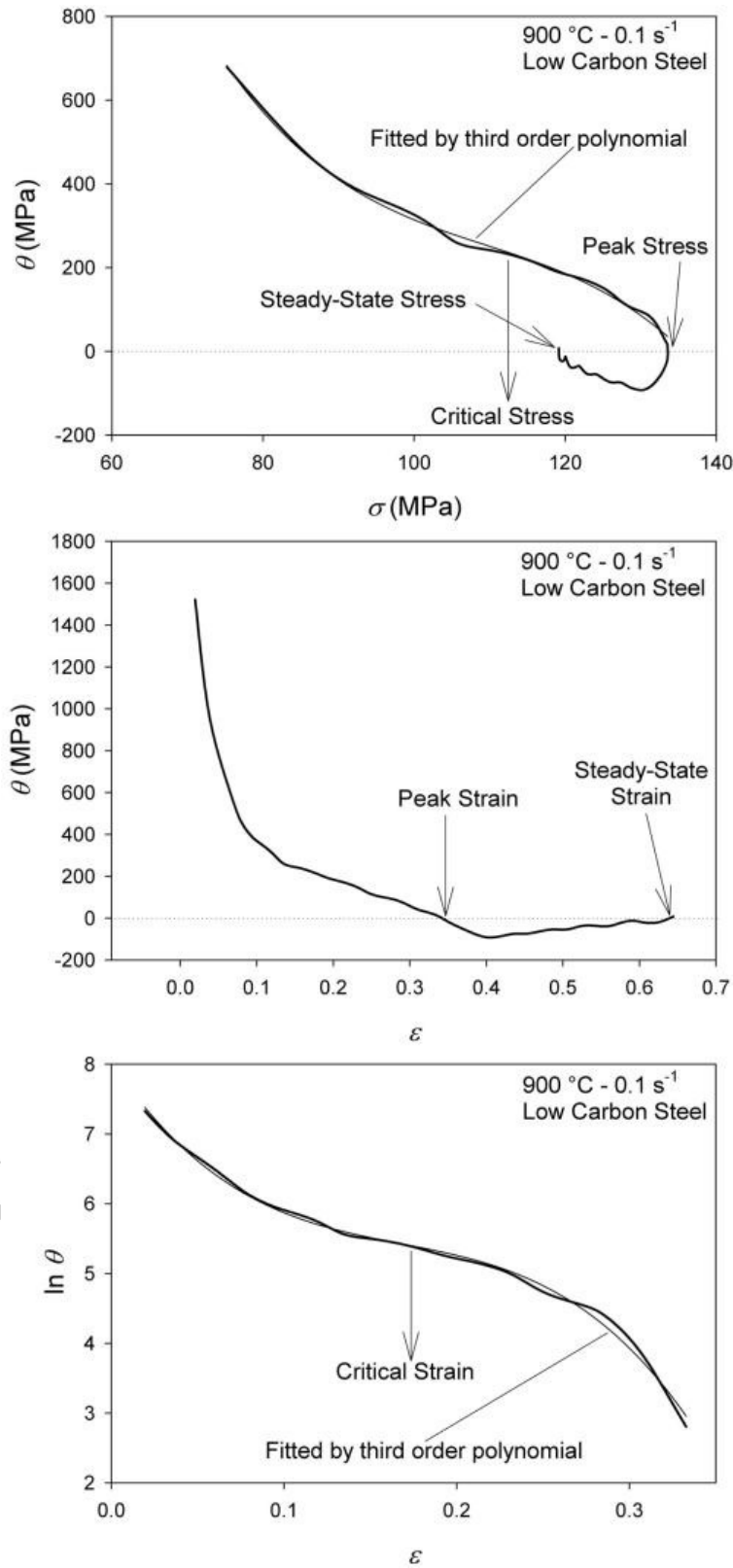
Fig. 3: Methods used for determination of characteristic points of flow curves.
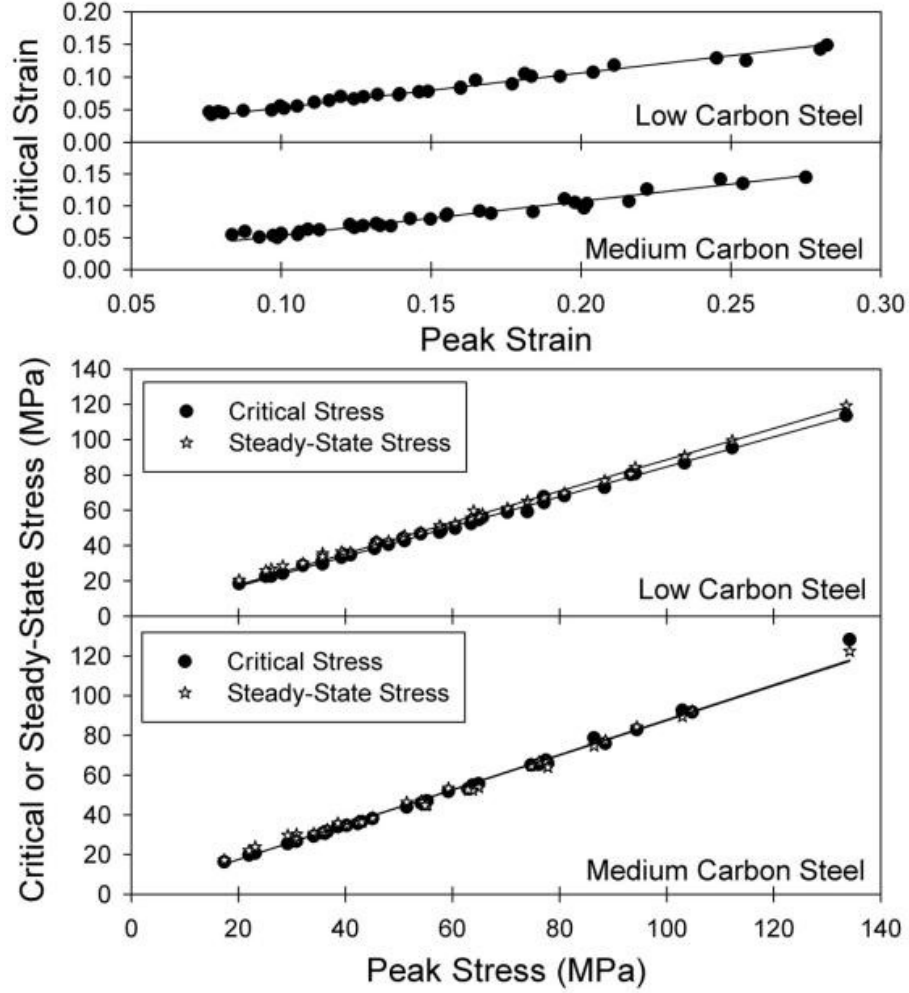
Fig. 4: Plots used to derive the relations among the various characteristic points of flow curves.

3.3. Constitutive modeling

One of the most-widely used parameters in hot deformation studies is the Zener-Hollomon one (Z),

which is also known as the temperature-compensated strain rate. The basic constitutive equations in

hot working are based on expressing Z as a function of flow stress as shown below [7,8]:

$$Z = \dot{\varepsilon} \exp\left(\frac{Q}{RT}\right) = \begin{cases} A' \sigma^{n'} \\ A'' \exp(\beta\sigma) \\ A[\sinh(\alpha\sigma)]^n \end{cases} \tag{2}$$

8

In this equation, Q is the hot deformation activation energy, $\dot{\varepsilon}$ is the strain rate, T is the absolute temperature, and finally A', A'', A, n', β, n, and α are material's parameters. The power law is preferred for relatively low stresses. Conversely, the exponential law is suitable for high stresses. Finally, the hyperbolic sine law can be used for a wide range of Z parameters. The stress multiplier α is an adjustable constant which brings $\alpha\sigma$ into the correct range that gives linear and parallel lines in $\ln\dot{\varepsilon}$ versus $\ln\{\sinh(\alpha\sigma)\}$ plots and it can be estimated by $\alpha \approx \beta/n'$.

By taking natural logarithm from both sides of the expressions of Eq. (2), the following expressions can be obtained:

$$\ln Z = \ln \dot{\varepsilon} + \frac{Q}{RT} = \begin{cases} \ln A' + n' \ln \sigma \\ \ln A'' + \beta \sigma \\ \ln A + n \ln[\sinh(\alpha\sigma)] \end{cases} \tag{3}$$

Since the deformation mechanism during hot working is usually based on the glide and climb of dislocations, the lattice self-diffusion activation energy can be employed as the deformation activation energy to determine Z [19]. As a result, the value of $Q_{SD} = 270$ kJ/mol [8,18] was considered for both steels in this work. Based on Eq. (3), the partial differentiation of the power and exponential laws leads to the following expressions at a given deformation temperature and for the particular case of the peak stress:

$$n' = [\partial \ln \dot{\varepsilon} / \partial \ln \sigma_P]_T \tag{4}$$

$$\beta = [\partial \ln \dot{\varepsilon} / \partial \sigma_P]_T \tag{5}$$

To determine the values of β and n' and subsequently, $\alpha \approx \beta/n'$, the slopes of the curves of $\ln\dot{\varepsilon}$ versus σ_p and $\ln\dot{\varepsilon}$ versus $\ln\sigma_P$ can be employed. These plots are shown in Fig. 5 and the values of α were

9

determined as 0.0183 and 0.0188 MPa^{-1} for low and medium carbon steels, respectively. Therefore, for comparison purposes, the value of α was taken as 0.018 for both steels. Plots of ln$Z$ vs. ln[sinh($\alpha\sigma$)] were employed to obtain the relations between σ_p and Z as shown in Fig. 6 and the resulting equations are indicated below:

$$Z = \dot{\varepsilon}\exp(\frac{270000}{RT}) = \begin{cases} 1.99\times10^8 \times[\sinh(0.018\sigma_P)]^{4.356} \Leftrightarrow 0.06\%C \\ 2.63\times10^8 \times[\sinh(0.018\sigma_P)]^{4.342} \Leftrightarrow 0.50\%C \end{cases} \qquad (6)$$
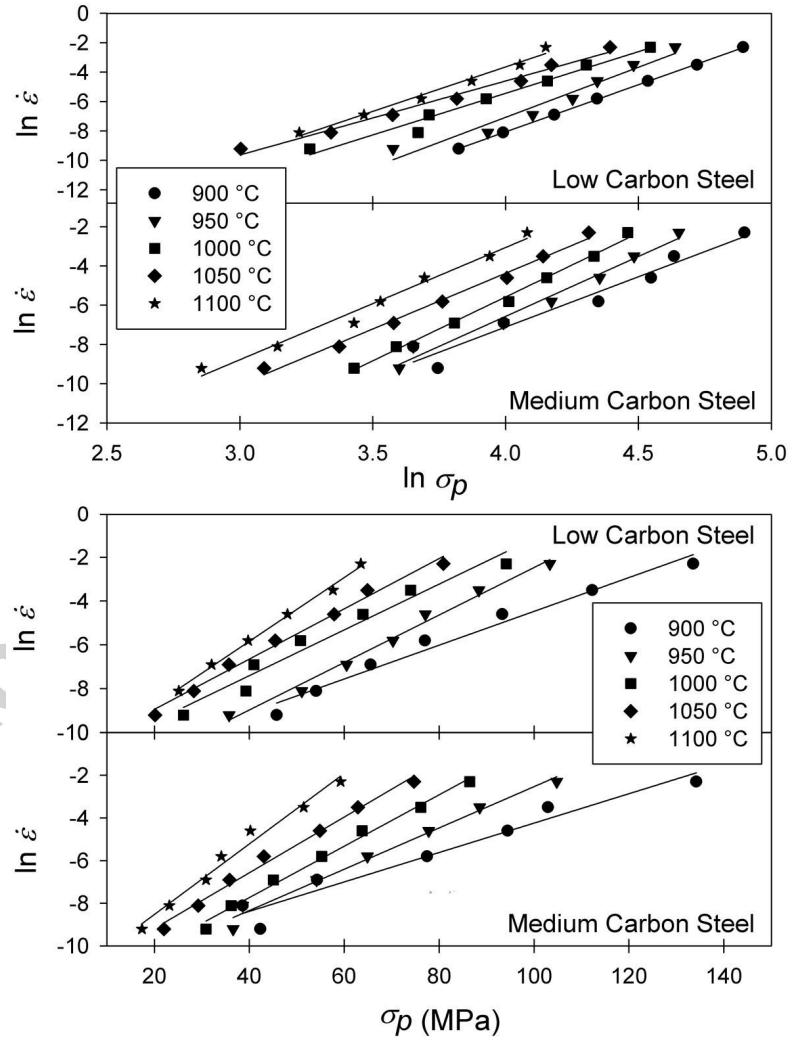

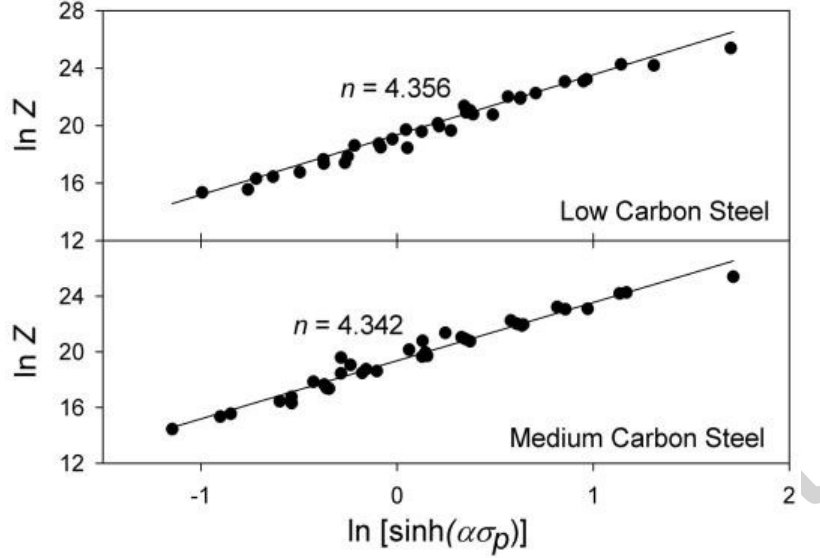Fig. 5: Plots used for determination of the stress multiplier α.

Fig. 6: Fitting the hyperbolic sine equation on the experimental data.

It can be seen that the value of *n* is near 4.5. It has been shown that the climb controlled intragranular flow of dislocations can be represented by $Q = Q_{SD}$ and *n'* or *n* = 4.5-5 [7-9,19-24]. Therefore, it can be deduced that the flow stress of the investigated materials during hot deformation is controlled by dislocation climb. To make the comparison possible, the theoretical value of *n* = 4.5 was considered for constitutive analysis and the results are shown in Fig. 7 and can be summarized as follows:

$$Z = \dot{\varepsilon}\exp(\frac{270000}{RT}) = \begin{cases} 1.97\times10^8 \times[\sinh(0.018\sigma_P)]^{4.5} \Leftrightarrow 0.06\%C \\ 2.60\times10^8 \times[\sinh(0.018\sigma_P)]^{4.5} \Leftrightarrow 0.50\%C \end{cases} \tag{7}$$

Since *n*, *α* and *Q* are the same for both steels, the only quantity to compare the flow stresses based on the hyperbolic sine law is *A*, which shows that the flow stress of the low carbon steel is somewhat higher than that of the medium carbon steel. This result is consistent with previous studies [11-13], which have shown that at low *Z* parameters, the flow stress of the plain carbon steels with higher amount of carbon is lower than in low carbon steels. This difference in the flow stress of the studied

11

materials can be understood by consideration of Eq. (8) as a result of rewriting Eq. (7), which shows that the level of the flow stress of low carbon steel at each Z is slightly higher than that of the medium carbon steel. This is also in accordance with some reports, which indicate that the flow stress of carbon steels at temperatures higher than 900 °C is almost independent of carbon content [10].

$$\sigma_P = \begin{cases} \sinh^{-1}\{0.01497 \times Z^{0.22}\}/0.018 \Leftrightarrow 0.06\%C \\ \sinh^{-1}\{0.01408 \times Z^{0.22}\}/0.018 \Leftrightarrow 0.50\%C \end{cases} \tag{8}$$
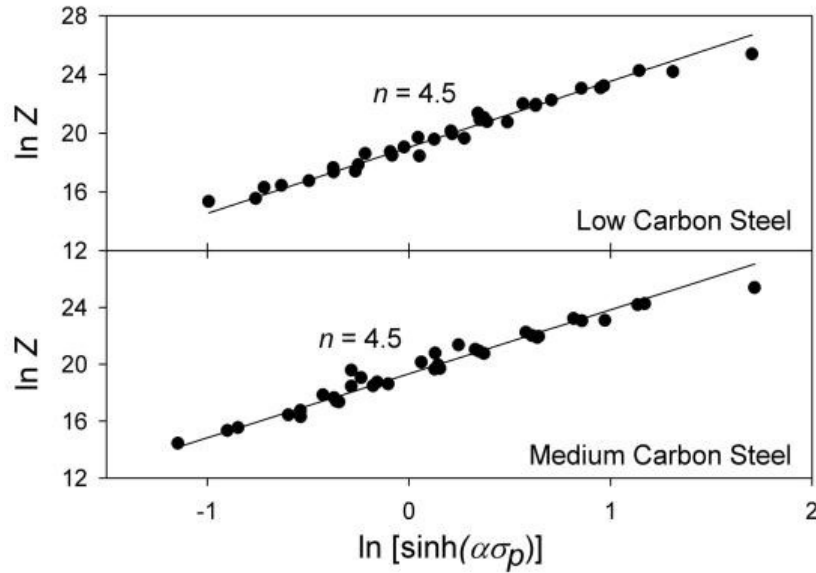

Fig. 7: Fitting the hyperbolic sine equation on the experimental data with $n = 4.5$.

In the aforementioned analysis, the value of Q was taken as Q_{SD} and it was shown that the flow stress of plain carbon steels can be adequately described by the climb controlled intragranular flow of dislocations. Here, the values of the apparent hot deformation activation energies will be obtained empirically to compare them with Q_{SD}. By partial differentiation of the hyperbolic sine expression in Eq. (3) at constant strain rate and also at constant temperature, the following relation will be resulted:

$$Q = R[\partial \ln \dot{\varepsilon} / \partial \ln[\sinh(\alpha\sigma_P)]]_T [\partial \ln[\sinh(\alpha\sigma_P)] / \partial(1/T)]_{\dot{\varepsilon}} \qquad (9)$$

Based on the abovementioned expression, the slope of the plot of $\ln[\sinh(\alpha\sigma_P)]$ vs. $1/T$ and the slope of the plot of $\ln\dot{\varepsilon}$ vs. $\ln[\sinh(\alpha\sigma_P)]$ were used to determine the value of Q. The related curves are depicted in Fig. 8, which resulted in the average values of 301.4 and 306.6 kJ/mol for the activation energies of medium and low carbon steels, respectively. It can be seen that these apparent values are nearly consistent with the theoretical value of $Q_{SD} = 270$ kJ/mol.
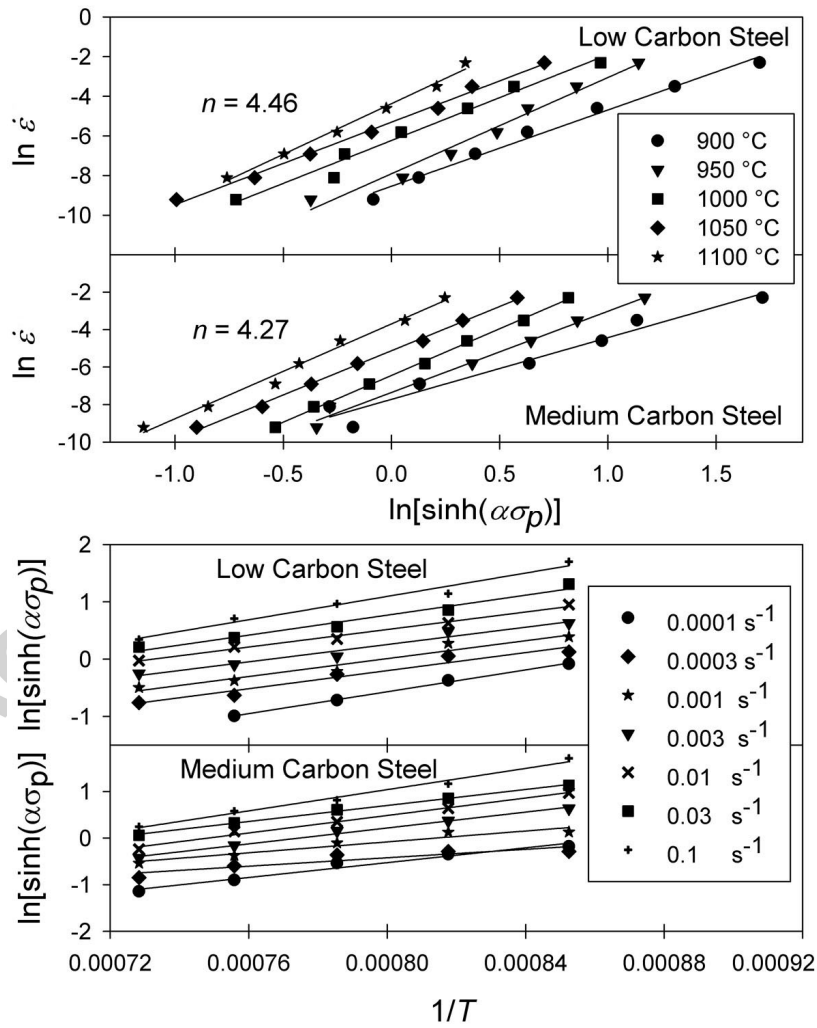

Fig. 8: Plots used for calculation of apparent deformation activation energies.

3.4. Characteristic points of flow curves vs. Z

Based on the power relation of $Z = A'\sigma_P^{n'}$, one can obtain an equation of the form of $\sigma_P = BZ^p$ to relate σ_P with Z. Similarly, the relation of $\varepsilon_P = CZ^q$ can be employed to find a relation between ε_P and Z. Therefore, the plots of $\ln\sigma_P$ and $\ln\varepsilon_P$ vs. lnZ can be used to find the values of B, p, C, and q. The required illustrations for both steels are shown in Fig. 9, which resulted in the following equations:

$$\sigma_P = \begin{cases} 1.85Z^{0.17} = 1.182\sigma_C \Leftrightarrow 0.06\%C \\ 1.75Z^{0.17} = 1.137\sigma_C \Leftrightarrow 0.50\%C \end{cases} \tag{10}$$

$$\varepsilon_P = \begin{cases} 0.0062Z^{0.155} = 1.883\varepsilon_C \Leftrightarrow 0.06\%C \\ 0.0123Z^{0.125} = 1.862\varepsilon_C \Leftrightarrow 0.50\%C \end{cases} \tag{11}$$

It follows from Eq. (10) that the level of peak flow stress for both steels is the same but the low carbon steel shows slightly higher flow stress. This small difference can be ascribed in part to the decreasing rate of work hardening due to enhanced dynamic recovery in the steel with higher carbon content as a result of expansion in the austenite lattice and enhanced diffusivity [11,12].

Since the Z exponents of Eq. (11) for the studied steels are different, the comparison cannot be made. Therefore, the direct relation between ε_C and Z is shown in Fig. 10, which displays that at the range of the deformation conditions used in this study, the level of ε_C for the medium carbon steel is higher than that of the low carbon steel ($\varepsilon_C|_{0.06\%C} = 0.93 \times \varepsilon_C|_{0.50\%C}$). This behavior is consistent with previous reports [13,14], which have indicated that at low Z values, the onset of DRX occurs at higher strains for the steels with higher carbon content. This delay in occurrence of DRX with increasing the carbon content can also be attributed to the enhanced dynamic recovery, which is the rival of recrystallization in consuming the stored energy, and hence, an enhancement in recovery can lead to reduction in driving force for the recrystallization process [6]. Based on Fig. 10, the

14

deformation conditions used in the present work belong to the low Z regime and it is anticipated that at lnZ higher than 25 (based on $Q = 270$ kJ/mol), a reverse trend is resulted, which is consistent with the observed trend in the previous research works [14]. However, It should be noted that the initial grain size for the low carbon steel is finer, which can decrease the values of the ε_C and ε_P. Therefore, the abovementioned comparison regarding the onset of DRX is not totally reliable. However, since the flow stress during hot deformation, resulted from the intragranular motion of dislocation, does not normally depend on grain size [19-21], the comparison regarding the flow stresses can be used safely.
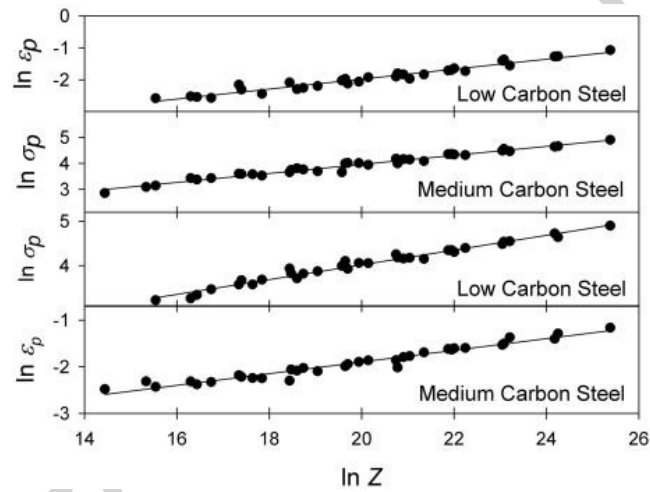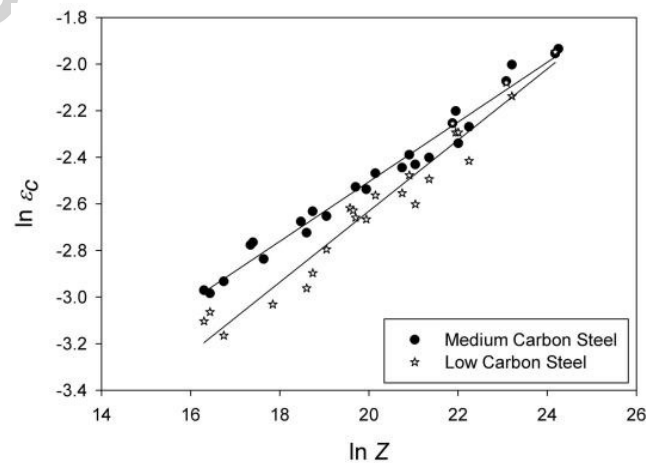

Fig. 9: The power law analysis.

Fig. 10: The critical strain for initiation of DRX *vs. Z.*

4. Conclusions

The following conclusions can be drawn from the study on the hot deformation behavior of plain carbon steels under the strain rate range of 10^{-4}-10^{-1} s^{-1} and temperature range of 900-1100 °C:

(1) Three types of dynamic recrystallization flow behaviors were identified, namely single peak, multiple transient steady state (MTSS), and multiple peak (cyclic) behaviors. The MTSS behavior was characterized as a transition state between single peak and cyclic behaviors. Moreover, the occurrence of this DRX flow behavior for plain carbon steels as well as stainless steels implies that the MTSS behavior might be a general flow behavior.

(2) The work hardening rate plots were used to determine the critical conditions for the onset of DRX and other characteristic points of flow curves. The normalized critical stress and strain for initiation of DRX were determined as $\sigma_C / \sigma_P = 0.879$ and $\varepsilon_C / \varepsilon_P = 0.537$ for medium carbon steel and $\sigma_C / \sigma_P = 0.846$ and $\varepsilon_C / \varepsilon_P = 0.531$ for low carbon steel, respectively. Therefore, it can be deduced that the onset of DRX in plain carbon steels takes place at normalized critical strain of ~ 0.53. The Z exponents for peak stress and strain were calculated as 0.17 and 0.125 for the medium carbon steel and 0.17 and 0.155 for the low carbon steel, respectively.

(3) The apparent deformation activation energies were determined as 301.4 and 306.6 kJ/mol for the medium and low carbon steels, respectively, which are near the lattice self-diffusion activation energy of austenite (Q_{SD} = 270 kJ/mol). The obtained hyperbolic sine powers were also close to 4.5, which signified that the flow stress of the investigated materials during hot deformation is controlled by the dislocation climb step. As a result, the following constitutive equations were proposed:

$$Z = \dot{\varepsilon}\exp(\frac{270000}{RT}) = \begin{cases} 1.97\times10^{8}\times[\sinh(0.018\sigma_P)]^{4.5} \Leftrightarrow 0.06\%C \\ 2.60\times10^{8}\times[\sinh(0.018\sigma_P)]^{4.5} \Leftrightarrow 0.50\%C \end{cases}$$

(4) Based on physically-based constitutive analysis, the difference between the flow stress of the medium and low carbon steels were related to the difference in the value of the hyperbolic sine

constant and it was found that carbon has a slight effect on the hot flow stress of plain carbon steels. This is important in term of deformation mechanisms without being based on the apparent material's constants and the obtained constitutive equations have a physical basis, which makes the comparison more reliable.

References

[1] Luton MJ, Sellars CM. Dynamic recrystallization in nickel and nickel-iron alloys during high temperature deformation. Acta Metall 1969;17:1033-1043.

[2] Mirzadeh H, Najafizadeh A, Moazeny M. Flow Curve Analysis of 17-4 PH Stainless Steel under Hot Compression Test. Metall Mater Trans A 2009;40A:2950-2958.

[3] Mirzadeh H, Najafizadeh A. Hot Deformation and Dynamic Recrystallization of 17-4 PH Stainless Steel. ISIJ Int 2013;53:680-689.

[4] Sakai T, Jonas JJ. Dynamic recrystallization: Mechanical and microstructural considerations. Acta Metall 1984;32:189-209.

[5] Dehghan-Manshadi A, Hodgson PD. Dynamic Recrystallization of Austenitic Stainless Steel under Multiple Peak Flow Behaviors. ISIJ Int 2007;47: 1799-1803.

[6] Humphreys FJ, Hatherly M. Recrystallization and related annealing phenomena. 2nd ed. Elsevier; 2004.

[7] Mirzadeh H. Quantification of the strengthening effect of reinforcements during hot deformation of aluminum-based composites. Mater Des 2015;65: 80-82.

[8] Mirzadeh H. Constitutive modeling and prediction of hot deformation flow stress under dynamic recrystallization conditions. Mech Mater 2015;85:66-79.

[9] Mirzadeh H. Constitutive analysis of Mg–Al–Zn magnesium alloys during hot deformation. Mech Mater 2014;77:80-85.

[10] Tamura I, Sekine H, Tanaka T, Ouchi C. Thermomechanical processing of High-strength low alloy steels. Butterworths; 1988.

[11] Wray PJ. Effect of carbon content on the plastic flow of plain carbon steels at elevated temoeratures. Metall Trans A 1982;13:125-134.

[12] Kong LX, Hodgson PD, Kollinson DC. Modelling the effect of carbon content on hot using a modified artificial neural network strength of steels. ISIJ Int 1998;38:1121-1129.

[13] Serajzadeh S, Karimi Taheri A. An investigation into the effect of carbon on the kinetics of dynamic restoration and flow behavior of carbon steels. Mech Mater 2003;35:653-660.

[14] Wray PJ. Effect of composition and initial grain size on the dynamic recrystallization of austenite in plain carbon steels. Metall Trans A 1984;15:2009-2019.

[15] Escobar F, Cabrera JM, Prado JM. Effect of carbon content on plastic flow behaviour of plain carbon steels at elevated temperature. Mater Sci Tech 2003;19:1137-1147.

[16] Poliak EI, Jonas JJ. A one-parameter approach to determining the critical conditions for the initiation of dynamic recrystallization. Acta Mater 1996;44:127-36.

[17] Mirzadeh H, Najafizadeh A. Prediction of the critical conditions for initiation of dynamic recrystallization. Mater Des 2010;31: 1174-1179.

[18] Mirzadeh H, Cabrera JM, Prado JM, Najafizadeh A. Hot deformation behavior of a medium carbon microalloyed steel. Mater Sci Eng A 2011;528:3876-3882.

[19] Mirzadeh H, Cabrera JM, Najafizadeh A. Constitutive relationships for hot deformation of austenite. Acta Mater 2011;59:6441-6448.

[20] Mirzadeh H. Constitutive behaviors of magnesium and Mg–Zn–Zr alloy during hot deformation. Mater Chem Phys 2015;152:123-126.

[21] Langdon TG. An Analysis of Flow Mechanisms in High Temperature Creep and Superplasticity. Mater Trans 2005;46:1951-1956.

[22] Mukherjee AK. An examination of the constitutive equation for elevated temperature plasticity. Mater Sci Eng A 2002;322:1-22.

[23] Mirzadeh H, Roostaei M, Parsa MH, Mahmudi R. Rate controlling mechanisms during hot deformation of Mg–3Gd–1Zn magnesium alloy: Dislocation glide and climb, dynamic recrystallization, and mechanical twinning. Mater Des 2015;68:228-231.

[24] Mirzadeh H. Constitutive description of 7075 aluminum alloy during hot deformation by apparent and physically-based approaches. J Mater Eng Perform 2015;24:1095-1099.

Figure Captions

Fig. 1: Flow curves obtained at different deformation conditions.

Fig. 2: Representation of different DRX flow curves for the medium carbon steel.

Fig. 3: Methods used for determination of characteristic points of flow curves.

Fig. 4: Plots used to derive the relations among the various characteristic points of flow curves.

Fig. 5: Plots used for determination of the stress multiplier α.

Fig. 6: Fitting the hyperbolic sine equation on the experimental data.

Fig. 7: Fitting the hyperbolic sine equation on the experimental data with $n = 4.5$.

Fig. 8: Plots used for calculation of apparent deformation activation energy.

Fig. 9: The power law analysis.

Fig. 10: The critical strain for initiation of DRX *vs. Z*.

Table Captions

Table 1 Chemical compositions (wt.%) of the studied plain carbon steels.

Table 1: Chemical compositions (wt.%) of the studied plain carbon steels.

Element	C	Mn	Si	P	S	Cu
Low Carbon Steel	0.06	0.42	0.12	0.002	0.005	0.13
Medium Carbon Steel	0.50	0.68	0.2	0.002	0.038	0.28